Direct Observation of Large Quantum Interference Effect in Anthraquinone solid state junctions

Vincent Rabache[†], Julien Chaste[†], Philippe Petit[†], Maria Luisa Della Rocca[†], Pascal Martin[§], Jean-Christophe Lacroix[§], Richard L. McCreery[‡], Philippe Lafarge[†]

[†] Université Paris Diderot, Sorbonne Paris Cité, MPQ, UMR 7162 CNRS, 10 rue Alice Domon et Léonie Duquet, 75205 Paris Cedex 13, France

[§] Université Paris Diderot, Sorbonne Paris Cité, ITODYS, UMR 7086 CNRS, 15 rue J-A de Baïf, 75205 Paris Cedex 13, France

[‡] National Institute for Nanotechnology, National Research Council Canada, Edmonton, Alberta, Canada, T6G 2M9

SUPPORTING INFORMATION

S1. Electroreduction of AQD

All chemical reagents were used as received. 9,10-dioxo-1-anthracenediazonium (AQD) was purchased from Acros Organics, ferricyanide of potassium ($K_3[FeCN_6]$) from Aldrich was used as redox probes. Tetrabutylammoniumtetrafluoroborate (Bu4NBF4) purchased from Aldrich at the highest available purity was used as supporting electrolyte at concentration 0.1 M in acetonitrile (ACN).

Figure S1 shows the 15th scan obtained on a gold electrode for the electroreduction of 9,10-dioxo-1-anthracenediazonium salt in ACN solution. At first cycle the irreversible wave corresponding to the reduction of diazonium salt is observed. Subsequent scans do not exhibit this peak. This is the typical behavior observed for the covalent grafting of gold with other aryl diazonium compounds[1].
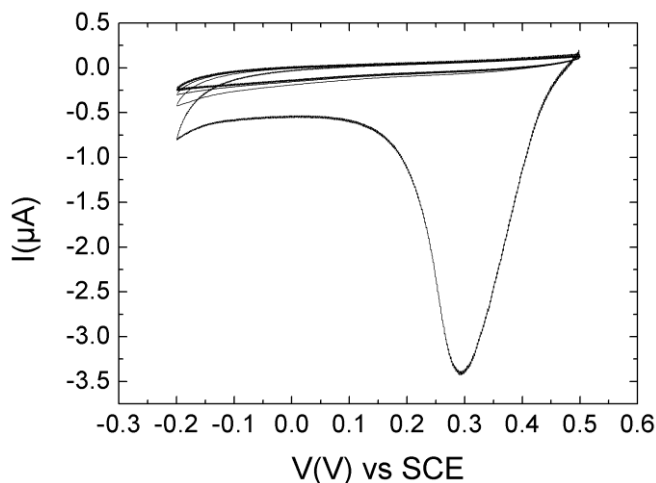
Figure S1. Cyclicvoltammograms of 9,10-dioxo-1-anthracenediazonium cation 5.10^{-3} M in ACN solution (0.1M Bu$_4$NBF$_4$) of on gold micro-electrode: 15th cycles. Scan rate 0.1 mV.s^{-1}

The presence of the anthraquinone layer was characterized by cycling the electrode in Ar-saturated 0.1 M KOH solution (Figure S2 and S3). The peaks in the voltammograms correspond

to the quinone/hydroquinone couple. The redox potential of surface anthraquinone was found to be -0.85 V.

Figure S2. Quinone/hydroquinone reaction in Ar-saturated 0.1M KOH solution.

The surface concentration of anthraquinone was determined by the charge integration under the cyclic voltammetry (CV) peaks ($\Gamma = \frac{Q}{nFA}$, where Q is the amount of charge consumed, n is the number of electron involved (n=2), F is the faraday constant and A is the area of electrode).
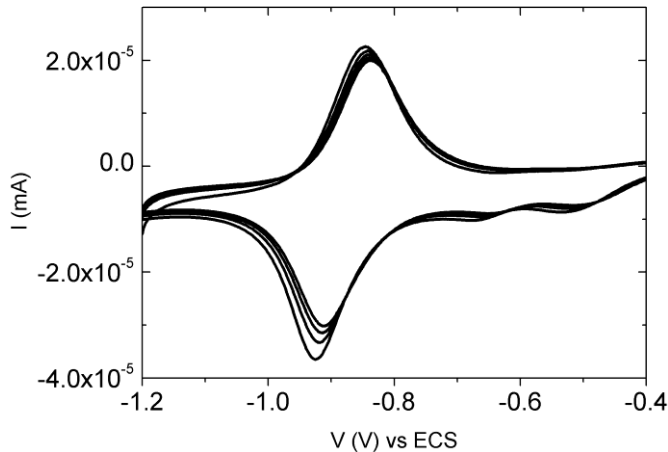
Figure S3. Cyclicvoltammograms of modified Au electrode in 0.1M KOH solution. Scan rate 0.1 mV.s^{-1}

In this work the surface coverage of AQ was around 2.1 x 10^{-9} mol.cm^{-2} for 15th cycles of grafting. It corresponds to more than one monolayer.

Cyclic voltammetry was also used to electrochemically test the blocking effect of anthraquinone (AQ) modified electrode towards the $Fe(CN)_6^{3-/4-}$ redox couple. The CV curves of

bare and modified electrodes in 5 mMK_3[FeCN$_6$] solution are presented in Figure S4. For 15th cycles, the CV response of redox probe is completely suppressed. Earlier studies have shown that for an effective electron transfer process Fe(CN)$_6^{3-}$ ions should interact with gold electrode[1]. This does not occur when a film completely covers the substrate surface. As a result the rate of electron transfer is strongly inhibited.
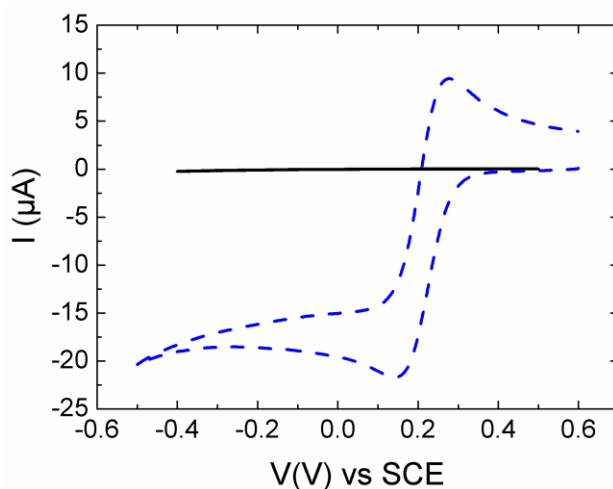
Figure S4. Cyclic voltammetry curves for a bare gold electrode (blue dotted curve) and for a AQ grafted electrode (black curve). The CV response of the grafted electrode is completely suppressed attesting the presence of the molecular layer covering the Au surface.

S2. Characterization of AQ layer

Surface morphology of anthraquinone modified gold electrodes was studied with AFM. Typical thopographical image of the AQ-modified electrodes is presented in Figure S5. It can be seen from the image that a uniform granular AQ film is formed on the electrode surface. The mean grain size is ~20 nm and the RMS roughness value is ~1.6 nm. Figure S5 (right) show an extracted section of the AQ layer for which the roughness mean value is ~1.3 nm .
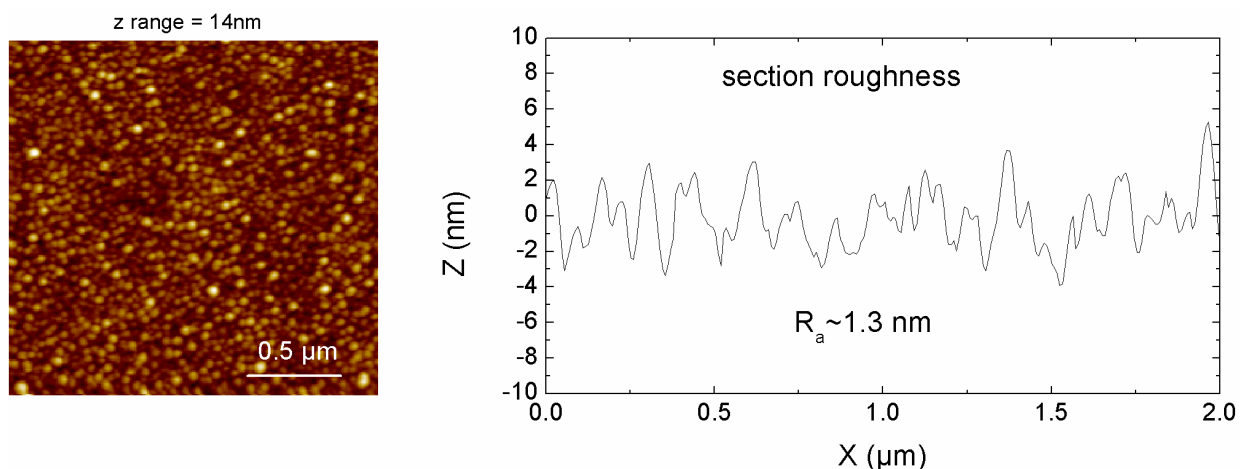
Figure S5. AFM image of a 2×2μm² area of anthraquinone grafted film covering a gold electrode (left). Extracted section showing a mean roughness value of ~1.3 nm (right).

An estimation of the AQ layer thickness has been obtained by comparing measurements of the

base electrode cross-section before and after grafting by AFM and profilometry.
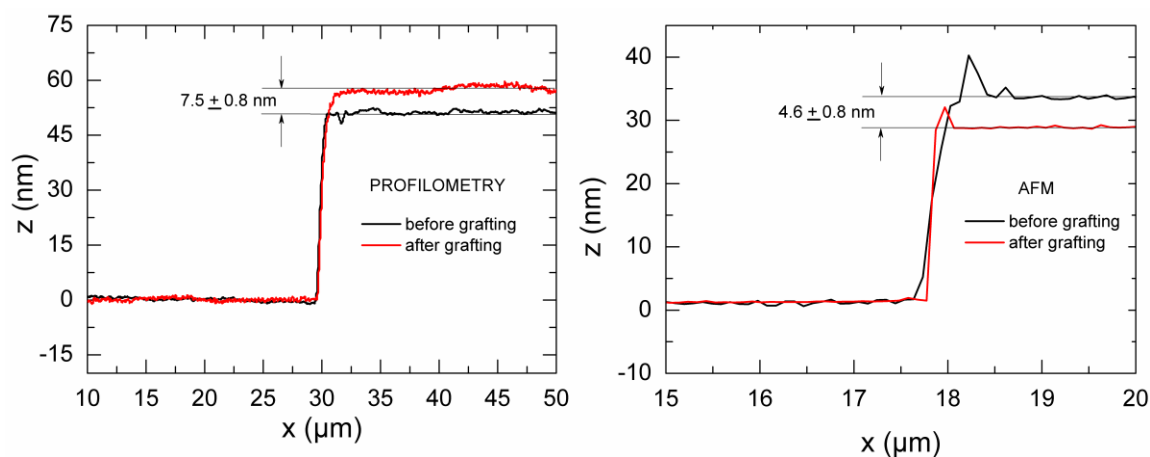
Figure S6. Partial cross section of Au electrode measured before and after gratfing on two different samples by profilometry (left) and AFM (right). Measurements correspond to a 15th and 10th cycling grafting procedure respectively.

Figure S6 show two different samples where grafting has been obtained by respectively 15th

and 10th voltammetry cycles. In the first case (left), the bare electrode has a thickness of ~50 nm

and, after grafting, a AQ layer of ~7.5 nm is revealed by profilometry. In the second case (right), the bare electrode has a thickness of ~27 nm and, after grafting, a AQ layer of ~4.6 nm is revealed by AFM. The AQ thickness is estimated beyond the intrinsic noise of the instruments. Samples analyzed on the main text have typically 10th voltammetry cycles, the thickness is therefore estimated at 4.6±0.8 nm.

S3. Measurements on other samples

In order to get a deeper insight into the interference effect manifested in AQ junctions, we conducted transport measurements using another electrode material than Au and with a linear-conjugated molecule. Figure S7 shows the $I(V)$ (a) and $dI/dV(V)$ (b) curves measured at 300K for 500×240 μm^2 area junctions in the case of an AQ (black circles) and AB (red triangles) molecular layers. The junctions have a carbon bottom electrode made of pyrolysed photoresist film (PPF) and a Cu/Au top electrode. As for the case of Au electrode, a typical V-shaped dip in the differential conductance is clearly visible for the AQ junction. In comparison the AB-based junction shows dI/dV curve with a parabola-like curvature typical of a tunnel junction behavior. Such differences in curve shapes are observed also in the $I(V)$ characteristics in Figure S7 (a). Asymmetries in the junctions with respect to zero voltage can be related to asymmetries in the electrode contacts. Surprisingly we find in the two cases comparable low bias conductance levels (dI/dV at $V = 0$), in contrast to what is typically observed in literature on different systems where a difference of 2-3 orders of magnitude in the low bias conductance distinguishes interfering form non-interfering junctions. We attribute this difference to the large area aspect of the junctions we fabricated, where we can easily have electronic paths not contributing to interferences but contributing to the total current in parallel with interfering paths.

Figure S8 show the log plot of *dI/dV* measurements taken at 4.2 K in a voltage range close to zero for 3 different junctions with area of 75×75 μm², 50×50 μm² and 30×30 μm² as indicated in the graphs. The conductance minimum is well defined and clearly oscillations structuring the dip are present. Where possible, oscillations which are symmetric with respect to zero voltage are indicated by vertical numbers bars.
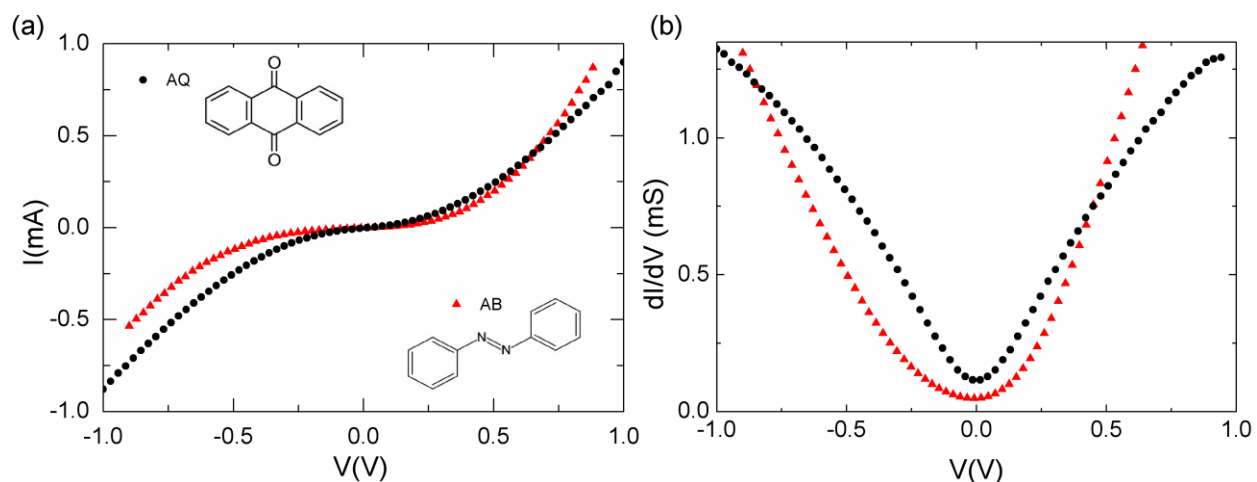
Figure S7. Measured *I(V)* (a) and d*I*/d*V(V)* (b) data at 300 K for AQ (black circles) and AB (red triangles) based junctions with a carbon bottom electrode and an area of 500×240 μm². A clear V-shaped anti-resonant dip is present only for the AQ-based junction as signature of quantum interference effects. In comparison the differential conductance of the AB-based junction has parabolic curvature typical of tunnel transport.
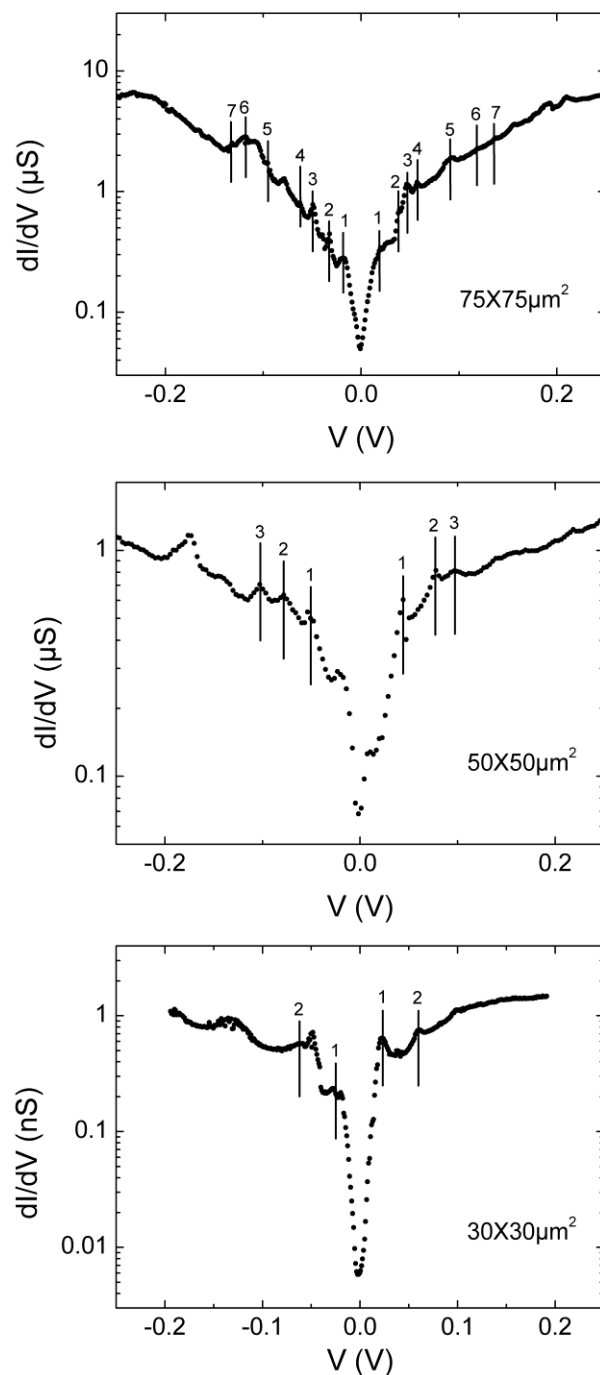
Figure S8. dI/dV for 3 different Au/AQ/Au junctions at 4K (junction area is indicated in the graph). A conductance minimum together with conductance oscillations is clearly evident at zero voltage. vertical numbered bars have been depicted to indicate oscillations peak positions symmetrical to zero voltage.

REFERENCES

(1) Chen, P.; McCreery, R.L. Anal. Chem*., Anal. Chem.* **1996**, *68*, 3958.